Nonlinear dynamics of a coupled micro-ring resonator chain

P. Chamorro-Posada,[1,*] P. Martin-Ramos,[1] J. Sánchez-Curto,[1] J.C. García-Escartín,[1] J.A. Calzada,[2]
C. Palencia[3] and A. Durán[3]

[1] Dpto. de Teoría de la Señal y Comunicaciones e Ingeniería Telemtica, Universidad de Valladolid,
ETSI Telecomunicación, Campus Miguel Delibes s/n, 47011 Valladolid, Spain.
[2] Dpto. de Matemática Aplicada, Universidad de Valladolid, ETSI Industriales,
Campus Miguel Delibes s/n, 47011 Valladolid, Spain.
[3] Dpto. de Matemática Aplicada, Universidad de Valladolid,
ETSI Telecomunicación, Campus Miguel Delibes s/n, 47011 Valladolid, Spain.
* Corresponding author: pedcha@tel.uva.es

Compiled December 16, 2010

We study nonlinear wave phenomena in a coupled ring resonator optical waveguide in the tight coupling regime. The discrete nonlinear Bloch modes of the structure are derived. The switching behavior of the transmission system is addressed numerically and the results are explained in the light of this analytical result. We also present a numerical study on the spontaneous generation of Bragg solitons from a continuous-wave input.

Transmission media consisting of chains of coupled micro-ring resonators find many applications in photonics. They have been proposed for the implementation of optical filters [1] or the realization of fast and slow wave structures [2–4]. One particular benefit of slow-wave optical systems is the associated enhancement of the nonlinear optical response [5,6]. In this letter, we study the nonlinear dynamics of a coupled resonator optical waveguide (CROW) built with micro-rings with a Kerr optical response.

Fig. 1. (a) Coupled ring resonator optical waveguide. (b) Unit cell of the resonator chain. (c) Band structure (first Brillouin zone) for a linear chain for $\theta = 0.5$ (solid) and $\theta = 0.8$ (dashed).

The CROW geometry is displayed in Figure 1.a. We will assume that the evanescent coupling between sections, with a phase jump of $\pi/2$ across the coupled waveguides, is localized at a single point and is described by the parameters θ and ρ, $\theta^2 + \rho^2 = 1$, as illustrated in Figure 1.b. We will neglect waveguide and material dispersion, since dispersive effects with origin in the resonator structure itself will dominate the former. The unit

cell defined in Figure1.b provides a discretization scheme for both space and time. The propagation length across one section is $L = \pi R$, with R is the resonator radius, and the sampling period is the corresponding propagation delay $\tau = L/v$, where v is the group (and phase) velocity in the optical waveguide sections. We consider a continuous-wave input with frequency ω and will denote with a superscript the time index, where instant k corresponds to $t_k = k\tau$. Thus, the complex field envelopes for the forward and backward waves in the structure at discrete position n and time k are $A_n^k = A_n(t_k)$ and $B_n^k = B_n(t_k)$, respectively.

The signal transmission across the cell length L has associated a linear phase $\exp(-j\Omega)$, with $\Omega = \omega L/v = \omega\tau$ and a linear loss factor $a = \exp(-\alpha L)$ where we assume a distributed loss with coefficient α. We will set $a = 1$ in the lossless case. The effect of the nonlinear phase will be computed along sections of length $d = L/2$. The nonlinear phase shift is $-\Gamma|E|^2$, where $\Gamma = \gamma d_{eff}$, γ is the nonlinear Kerr coefficient and $d_{eff} = (1 - exp(-\alpha d))/(2\alpha)$.

The discrete spatio-temporal dynamics are then described as

$$
\begin{aligned}
A_n^{k+1} = a \Big[& j\theta A_{n-1}^k \exp\left(-j\Gamma \left|A_{n-1}^k\right|^2\right) + \\
& \rho B_n^k \exp\left(-j\Gamma \left|B_n^k\right|^2\right) \Big] \exp(-j\Omega) \exp\left(-j\Gamma \left|A_n^{k+1}\right|^2\right) \\
B_n^{k+1} = a \Big[& j\theta B_{n+1}^k \exp\left(-j\Gamma \left|B_{n+1}^k\right|^2\right) + \\
& \rho A_n^k \exp\left(-j\Gamma \left|A_n^k\right|^2\right) \Big] \exp(-j\Omega) \exp\left(-j\Gamma \left|B_n^{k+1}\right|^2\right).
\end{aligned}
\tag{1}
$$

Equations (1) can be written in time-explicit form substituting

$$
\left|A_n^{k+1}\right| = a \left| j\theta A_{n-1}^k \exp\left(-j\Gamma \left|A_{n-1}^k\right|^2\right) + \rho B_n^k \exp\left(-j\Gamma \left|B_n^k\right|^2\right) \right|
$$

$$
\left|B_n^{k+1}\right| = a \left| j\theta B_{n+1}^k \exp\left(-j\Gamma \left|B_{n+1}^k\right|^2\right) + \rho A_n^k \exp\left(-j\Gamma \left|A_n^k\right|^2\right) \right|
\tag{2}
$$

in the last exponential terms in Eqs. (1). Even though we will restrict the analyses to the lossless case $a = 1$, these structures typically exhibit a certain amount of intrinsic radiation loss [7] dependent on the refractive index contrast of the guiding structures. Moreover, we have found in the numerical simulations that propagation losses have the expected result of stabilizing to some extent the signal transmission. The in-depth study of the effect of loss will be the subject of a forthcoming publication.

The steady state response for a 1-ring CROW has been shown to exhibit transmission bistability [4] and multistability has been reported for the N-ring system [9]. Even for an isolated resonator, the micro-ring will display a Ikeda-type instability [10] and behave as a chaotic oscillator [11]. The CROW can be described as a coupled array of such oscillators and, not surprisingly, the numerical simulations often show a chaotic response when the system is driven to highly nonlinear regimes. Therefore, we will restrict our analyses to a tightly coupled micro-ring chains, $\theta \to 1$, where signal transmission across resonator stages is large and, thus, stable (nonlinear) propagation effects can be efficiently addressed. Regarding the transverse instabilities of the type described in [12], we have already assumed that the size of the micro-rings is too small for these to be of any relevance when neglecting material or waveguide dispersion.

Signal propagation in the CROW can be analyzed drawing a discrete Floquet-Bloch theory for the CROW model (1) analogue to that of continuous periodic systems [14]. For an infinite chain, we consider steady-state solutions for the complex envelopes of the type

$$A_n = A \exp\left(-jnQ\right), \ B_n = B \exp\left(-jnQ\right), \quad (3)$$

characterized by the mode wave-number Q. For the linear case, we set $\Gamma = 0$ in Eqs. (1) and obtain the linear dispersion relation

$$\cos Q = \sin \Omega/\theta, \quad (4)$$

which provides a relation between Q and Ω that is periodic in both variables. Figure 1.c shows the first Brillouin zone ($Q \in [-\pi, \pi]$) for two different values of θ. The dispersion relation gives linear Bloch wave-numbers Q which become imaginary in a range of Ω values defined by the condition $\sin \Omega/\theta > 1$. These regions, where signal propagation is forbidden, define the bands that are highlighted in Fig. 1.c. We will focus our analysis on the second forbidden band in Fig. 1 at the edge of the first Brillouin zone $Q = \pi$. The band-gap spans the interval $[\Omega_1, \Omega_2]$ with $\Omega_1 = 2\pi - 2\arcsin(\theta)$ and $\Omega_2 = 2\pi - \arcsin(\theta)$. Figure 1 also illustrates the narrowing of the bands as θ increases, which results in a very narrow gap when we approach the tightly-coupled limit $\theta \to 1$.

We define $P = |A|^2 + |B|^2$ and the amplitude ratio $f = B/A$. The mode amplitudes can be expressed as $|A| = \sqrt{P/(1 + |f|^2)}$ and $|B| = |f|\sqrt{P/(1 + |f|^2)}$. Substitution of (1) into (3) gives the nonlinear dispersion relation

$$\cos\left(Q + \Delta Q\right) = \sin\left(\Omega + \Gamma P\right)/\theta, \quad (5)$$

where $\Delta Q = \Gamma P(|f|^2 - 1)/(|f|^2 + 1)$. $|f|$ can be obtained as a solution of the implicit equation

$$|f| = \rho \left(1 + \theta^2 \exp(-2q_I) - 2\theta \exp(-q_I)\sin(q_R + \Delta Q)\right)^{\frac{1}{2}} \quad (6)$$

with $Q = q_R - iq_I$; q_R and q_I are real. In the nonlinear case, Q is real out of the forbidden bands and has non-zero real and imaginary parts otherwise (except for $|f| = 1$). In this regime, $q_R = -\Delta Q$ and

$$q_I = \cosh^{-1}\left(\sin(\Omega + \Gamma P)/\theta\right). \quad (7)$$

Thus, nonlinearity has the effect of shifting the dispersion relation and the whole band structure in the ΩQ plane. An input signal with a frequency inside a forbidden band will experience a transmission attenuation dependent on the propagation nonlinearity as the imaginary part of Q is modified according to (7). This mechanism explains the switching behavior of this type of structures [13], where a change in the attenuation constant of the propagating signal will produce a corresponding variation of the transmitted signal amplitude.

We have addressed the switching effect numerically by placing a unit amplitude input signal $|A_1| = 1$ with a frequency $\Omega = 3\pi/2$ (in the middle of the second forbidden band) for different values of Γ. This is fully equivalent to keeping Γ constant and changing the input amplitude accordingly. We have also checked that identical dynamics are produced when the input frequency is tuned to the middle of the first band $\Omega = \pi/2$. The numerical solutions are obtained with a computer code designed for more general propagation conditions [3, 4] which allows for signal fluctuations at a scale smaller than τ, but comprises any result from the model equations (1) whenever the dynamics are kept within the time scale τ, which will be always the case for the results presented in this work.
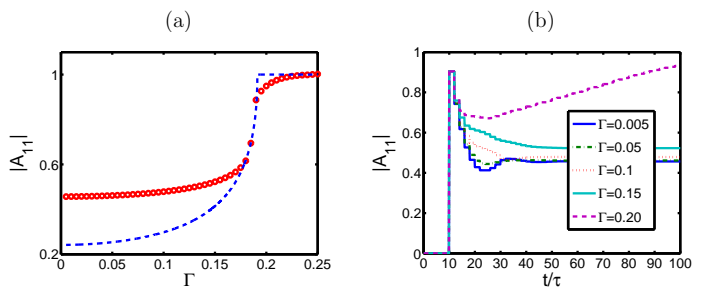

Fig. 2. (a) Nonlinear switching in a $N = 10$ CROW with $\theta = 0.99$ as obtained numerically (points) and fitted prediction from the nonlinear dispersion relation (7) assuming the absence of boundary effects (dashed). (b) Transient output response for five values of Γ.

There are two effects that have not been accounted for in the derivation of the exact nonlinear Bloch modes

but are present in the actual system dynamics. For finite length structures, boundary effects will result in the excitation of backward propagating $(A_n^-, B_n^-) = (A^-, B^-)\exp(jnQ)$ Bloch modes. Furthermore, the presence of a counter-propagating wave has not been considered in the derivation of the exact Bloch mode solution, but will modify the propagation properties.

In our numerical experiments, we are imposing the boundary conditions $A_1^k = \exp(-j\Omega k)$ and $B_{N+1}^k = 0$. The condition at $N + 1$ is expected to produce an ideal reflection of the Bloch wave at the end of the structure, whereas the input condition at $n = 1$ effectively fixes the forward wave in the steady state since the contributions of subsequent reflections will be largely attenuated.

In Figure 2.a the numerical results of the transmission switching are displayed with points. In order to illustrate the qualitative switching behavior predicted by the analytical model, the results for a forward propagating Bloch mode $A_{N+1} = A_1 \exp(-jQN)$ are shown with a dashed line. Q is obtained from Equation 7 fitted with a particular value of P. Even though the analytical model does not encompass the full complexity of the nonlinear problem in the presence of reflected nonlinear Bloch waves, it still provides a good qualitative description of the switching behavior. The numerical results in Figure 2.a show that for very low nonlinearity, the total output amplitude is very close to the double of the value of $|A_{N+1}|$ that would result from a perfect reflection of the attenuated linear mode. Figure 2.b shows the output transient for various values of Γ.
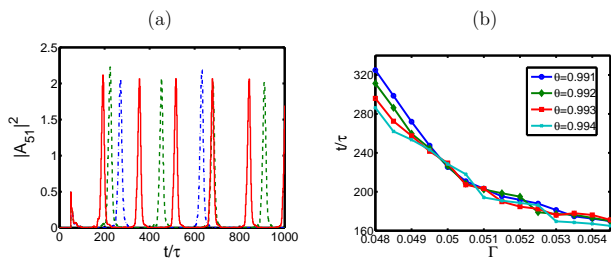

Fig. 3. (a) Spontaneously generated pulse trains for $\theta = 0.993$ and $\Gamma = 0.047$ (dashed-dotted), $\Gamma = 0.050$ (dashed) and $\Gamma = 0.055$ (solid). Pulse repetition period for varying Γ and four values of θ.

Inside the forbidden band, close the band edge, the dynamics are known to be well-described by a nonlinear Schrödinger equation [15, 16]. It is anticipated that the nonlinear Bloch soliton solutions are modulationally unstable for sufficiently high nonlinearity and that Bragg solitons [17, 18] arise as attractors of the nonlinear dynamics. We address numerically this effect for a chain with $N = 50$ cells in the tight-coupling regime $\theta \to 1$ by tuning the input frequency to a ten percent of the total frequency gap inside the forbidden band in each case. Figure 3.a illustrates typical pulse sequences obtained after the onset of the instability. For these simulations, the intra-cavity field displays the expected generation and

subsequent propagation of a soliton inside the CROW. Also, one can observe in Figure 3.a how the pulse spacing decreases as the nonlinearity increases. This effect is illustrated in Figure 3.b for four different values of θ and values of Γ in the range between 0.048 and 0.054.

In summary, we have presented a study of the nonlinear wave propagation phenomena displayed by a nonlinear CROW. A model for the system dynamics has been introduced and its exact nonlinear Bloch modes have been derived. Also, we have numerically studied the generation of Bragg solitons in the structure. Further analyses for the system behavior in the presence of propagation loss and the linear stability analysis to analytically predict the instability threshold will be addressed in future publications.

References

1. J. Capmany, P. Muñoz, J.D. Domenech and M.A. Muriel, "Apodized coupled resonator waveguides," Opt. Express **15**, 10196–10206 (2007).
2. J.E. Heebner and R.W. Boyd, "Slow and fast light in resonator-coupled waveguides," J. Mod. Opt. **49**, 2629-2636 (2002). Photonics News 17, 18 (2006).
3. P. Chamorro-Posada and F.J. Fraile-Pelaez, "Fast and slow light in zigzag microring resonator chains," Opt. Lett. **34**, 626-628 (2009).
4. F.J. Fraile-Peláez and P. Chamorro-Posada, "Active control and stability in microring resonator chains," Opt. Express **15**, 3177–3189 (2007).
5. Y. Chen and S. Blair, "Nonlinearity enhancement in finite coupled-resonator slow-light waveguides," Opt. Express **12**, 3353–3367 (2004).
6. A. Melloni, F. Morichetti and M. Martinelli, "Linear and nonlinear pulse propagation in coupled resonator slow-wave optical structures," Opt. Quantum Electron. **35**, 365–379 (2003).
7. P. Chamorro-Posada and F.J. Fraile-Peláez, "Superluminal propgation in resonant dissipative media," Opt. Commun. **282**, 1095–1098 (2009).
8. F.J. Fraile-Peláez, J. Capmany and M.A. Muriel, "Trasmission bistability in a double-coupler fiber ring resonator," Opt. Lett. **16**, 907–909 (1991).
9. Y. Dumeige, L. Ghisa and P. Feron, "Dispersive multi-stability in microring resonators," J. Opt. A: Pure Appl. Opt. **8**, S483–S489 (2006).
10. K.Ikeda, H. Daido and O. Akimoto, "Optical Turbulence: Chaotic Behaviour of Transmitted Light from a Ring Cavity," Phys. Rev. Lett. **45** 709–712 (1980).
11. M. Prol, F.J. Fraile-Peláez, R. Gomez-Alcalá, P. Chamorro-Posada and D.J. Santos, "Instability and chaos in a two-coupler fiber ring resonator," Fiber Integrated Opt. **14**, 331-335 (1995).
12. D.W. McLaughlin, J.V. Moloney and A.C. Newell, "New Class of Instabilities in Passive Optical Cavities," Phys. Rev. Lett. **54**, 681–682 (1985).

13. N.G.R. Broderick, D. Taverner and D.J. Richardson, "Nonlinear switching in fibre Bragg gratins," Opt. Express **3**, 447–453 (1998).
14. Y.S. Kivshar, *Optical Solitons: From Fibers to Photonic Crystals* (Academic Press, 2003).
15. I. Neokosmidis, T. Kamalakis and T. Sphicopoulos, "Optical Dealy Lines Based on Soliton Propagation in Photonic Crystal Coupled Resonator Optical Waveguides," IEEE J. Quantum Electron. **43**, 560–567 (2007).
16. B.J. Eggleton, C. Martijn de Sterke and R.E. Slusher, "Bragg solitons in the nonlinear Schrödinger limit: experiment and theory," J. Opt. Soc. Am. B **16**, 587–599 (1999).
17. D.N. Christodoulides, R.I. Joseph, "Slow Bragg Solitons in Nonlinear Periodic Structures," Phys. Rev. Lett. **62**, 1746–1749 (1989).
18. A.B. Aceves and S. Wabnitz, "Self-induced transparency solitons in nonlinear refractive periodic media," Phys. Lett. A **141**, 37–42 (1989).